

Image analysis application for automatic quantification of intramuscular connective tissue in meat

F.G. Del Moral^a, F. O'Valle^a, M. Masseroli^b, R.G. Del Moral^{a,*}

^a Department of Pathology, School of Medicine, University of Granada, 18012 Granada, Spain

^b Department of Biomedical Engineering, Politecnico di Milano, Piazza Leonardo da Vinci 32, I-20133 Milano, Italy

Abstract

An image analysis application for the quantification of meat intramuscular connective tissue (IMCT) and fibre retraction is presented. This image analysis method was applied to microscopic images of Sirius red-stained tissue sections from various animal species (pig, cow, pigeon, and lamb), including different breeds of pig (Large White crossbreed and Iberian) and cow (Kobe and Rubia Gallega). Results obtained showed statistically significant differences among the species in area and percentage of IMCT, *perimysium* and fibre retraction in meat ($p < 0.001$, Kruskal–Wallis). Significant differences were also observed between the two breeds of pig in percentages of IMCT (4.00 ± 2.15 vs. 17.02 ± 14.99 ; $p = 0.028$, Mann–Whitney U test) and *perimysium* (22.59 ± 0.87 vs. 9.93 ± 4.95 ; $p = 0.009$, Mann–Whitney U test) in *longissimus thoracis* (LT). This original design software permits the accurate, objective, reliable, and fully reproducible quantification of IMCT and fibre retraction in meat.

Keywords: Image analysis; Sirius red; Intramuscular connective tissue; *Perimysium*; Muscle fibre retraction; Meat; Beef; Kobe beef; Pork; Iberian pork; Pigeon; Lamb

1. Introduction

Image analysis was recently described as a highly promising approach for objectively assessing meat freshness and for the on-line quality control of industrial meat products (Du & Sun, 2004; Ötles & Önal, 2004; Swatland, 1995; Wyle et al., 2003). In fact, it has been used since the early 1980s (Cross, Gilliland, Durland, & Seideman, 1983; Wassemberg, Allen, & Kemp, 1986) to determine crude fat content, colour, lean yield estimate, marbling and textural properties and to relate these results to the palatability and tenderness of cooked meats (Tan, 2004; Vote, Belk, Tatum, Scanga, & Smith, 2003).

The search for meat tenderness has long captured the attention of research groups and meat producers. Chandraratne et al. (2005) define the tenderness of meat as its

resistance to shear, or toughness. Many studies have focussed on muscle fibre, but there has also been considerable investigation of intramuscular connective tissue (IMCT), which has been shown to be a critical factor in meat tenderness. Swatland (2006) concluded that the strength of the strongest *perimysium* in aged beef roasts is more than twice the sum of the endomysial and myofibrillar strength. In a recent review of IMCT studies, Purslow (2005) reported the morphology, composition and amount of IMCT vary enormously among muscles, species, breeds and animals of different ages.

Studies of IMCT by imaging analysis and microscopy have recently been published, notably by Sifre et al. (2005) and Sifre-Maunier, Taylor, Berge, Culioli, & Bonny (2006). These authors accepted the equivalent importance of the two main structural constituents of muscle tissue (myofibres and IMCT) and concluded that structural studies were required to predict meat tenderness and instrumental toughness. According to Sifre-Maunier et al. (2006), if

the contribution of the myofibres to meat toughness is limited by proper post-mortem handling, the contribution of the IMCT predominates, especially after an adequate ageing period, and the feature of IMCT is mostly determined by the amount and heat solubility of collagen and its spatial organisation in the muscle.

These studies have opened up a highly productive line of research into the architecture of IMCT and the possibility of obtaining highly precise and objective measurements based on microscopy and imaging analysis.

This paper presents a new automatic image analysis method based on digital analysis designed to quantitatively study the area of IMCT and fibre retraction in Sirius-red and hematoxylin–eosin-stained histological sections of meat, respectively. This software, originally designed for biomedical applications, permits the accurate, objective, reliable, and fully reproducible quantification of areas of IMCT or muscle fibre retraction in meat and enables assessment of other parameters not adequately studied to date.

2. Materials and methods

2.1. Animals

A total of 30 male animals were studied. Five each of commercially available Large White crossbreed pigs (100–110 kg), Iberian pigs (160–175 kg), lamb (9–11 kg), Rubia Gallega cows (around 450 kg), Kobe steers (550–570 kg) and pigeons (0.45–0.50 kg) were raised in Spain under standard commercial production systems and subjected to normal husbandry practices. In Iberian pigs, a traditional “hot deboning” was applied to carcasses and sampling was carried out within one hour after slaughter.

2.2. Histologic study

Five transverse histologic sections ($2 \times 2 \times 0.5$ cm) of raw muscle tissue were taken from each animal, from *longissimus thoracis* (LT) (at 10th rib of pork, beef, and lamb), *masseter* (M, beef), *triceps brachii* (TB, lamb) and *pectoralis major* (PM, pigeon). Tissues were fixed in buffered 4% formalin (Panreac, Barcelona, Spain) and embedded in paraffin; 4- μ m sections were kept after deparaffinization for 48 h in 70% alcohol before their simultaneous staining with 1% micro Sirius red F3BA (Gurr, BDH Chemicals Ltd., Poole, United Kingdom) for 30 min. Using Sirius red, connective tissue is stained a deep red colour and nuclei and cytoplasmic muscle structures are stained light red and bright yellow, respectively (Sweat, Puchtler, & Rosenthal, 1964). This staining was used to assess area and percentage of *epimysium*, *perimysium*, *endomysium*, i.e., the main components of IMCT. Serial sections were also stained using standard hematoxylin–eosin technique to evaluate the extent of muscle fibre retraction.

2.3. Image analysis morphometric study

2.3.1. Image capture

Seventy-five images per sample were captured with a black and white Vidamax CCD BCD-700 video camera (ImaGesp, Barcelona, Spain) coupled to an Olympus BH-2 microscope (20 W) with MTV-3 adapter (Olympus Optical Company, Ltd., Tokyo, Japan). Use of an intermediate lens ($3.3\times$) and $10\times$ or $20\times$ power objectives yielded a total magnification of $100\times$ or $200\times$, respectively. Analog images were captured through an IF 550 green optical filter (Olympus) and digitized at 8 bits intensity resolution (256 grey levels). For all measurements, the light intensity of the microscope was set at 7, video camera gain was 230, focus aperture was completely open and camera offset was set at 0. The diaphragm aperture was 0.25 for muscle fibre retraction quantification, 0.20 for IMCT and 0.32 for *perimysium*. In all cases, the images were captured with light overexposure to increase contrast and eliminate areas with grey levels close to white.

2.3.2. Image processing

The image analysis system consisted of a PC with Pentium-4, 3.20 GHz processor, 1 Gbytes Ram, S-VGA 1 Mbyte graphics card, Meteor II/Standard MPEG card (Matrox Electronics System, Ltd., Dorval, Canada) for image capture and processing, and a FLATRON L1730S monitor (LG, Seoul, Korea). Image processing and computer operations were performed in Windows XP Professional environment (Microsoft Corporation, Redmond, Washington) with original algorithms implemented using Visilog 6.0 software (Noesis S.A. Courteboeuf, France) for the development of image analysis programmes with programme compiler in C language: Turbo C 2.0 (Borland International Inc.).

2.4. Statistical analysis

The Kolmogorov–Smirnov test was used to assess the normal distribution of the variables. After the descriptive analysis, Spearman correlation (ρ), Kruskal–Wallis, and Mann–Whitney U test analyses were performed to determine the statistical significance. The confidence interval was 95% ($p < 0.05$). The statistical analysis was performed using the SPSS-Windows 11.0 programme (SPSS Inc., Chicago, USA).

3. Results and discussion

3.1. Programme

A computer programme was adapted for the automatic quantification of IMCT and fibre retraction in microscopic images of meat tissue. The application consisted of the following modules (Fig. 1): automatic capture, automatic thresholding, morphologic filtering algorithm, IMCT area identification and image analysis.

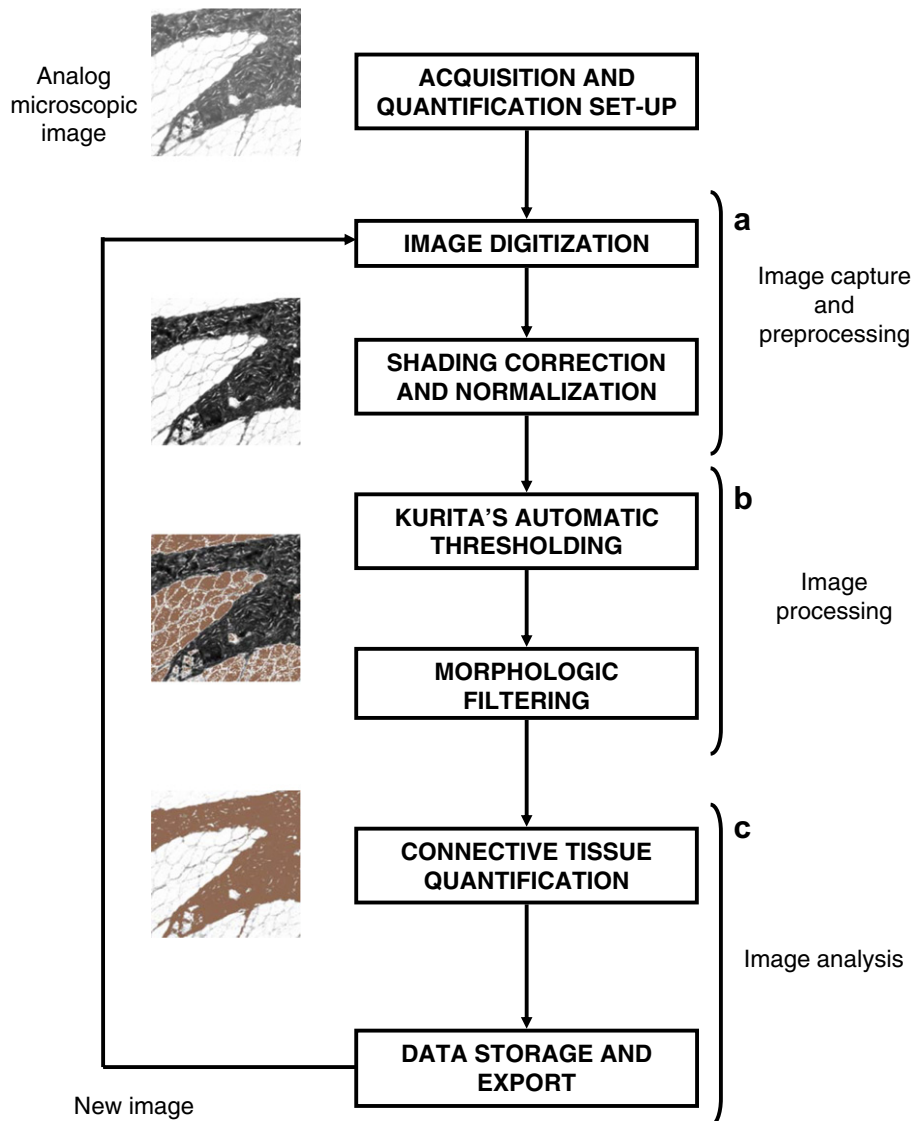


Fig. 1. Flow chart of image analysis application for automatic quantification of IMCT, showing main components of the image analysis application developed to automatically quantify intramuscular connective tissue in meat sections. The programme is implemented in three parts: (a) capture and pre-processing of digital image, (b) processing of pre-processed image, and (c) analysis of processed image and measurement of parameters. Black-white microscopic images of M of Rubia Gallega beef (Sirius red, $\times 10$).

3.1.1. Automatic capture

This enables capture and improvement of the microscopic image by removing grey levels of the preparation in areas without tissue and normalizing the grey histogram of the image, highlighting Sirius red- or hematoxylin-eosin-stained connective tissue areas. To avoid interference causing by irregular lighting and camera lens aberrations, the shading in the digitized image was corrected by comparing the image pixel-by-pixel with a previously acquired background image and the corrected image was then normalized.

3.1.2. Automatic thresholding

Automatic segmentation of areas intensely stained by Sirius red or hematoxylin-eosin was carried out using the

global thresholding method of Kurita, Otsu, and Abdelmalek (1992). In images of meat stained with Sirius red, captured with excess light and pre-processed as previously described, thresholding yielded a binary image representing the extracellular matrix of the muscle interstitium (made up of different types of collagen and nonfibrillar proteins) and the muscle cells. A second algorithm using Kittler and Illingworth thresholding (Kittler & Illingworth, 1986) was implemented on the initial image for detecting lower grey levels, in order to isolate areas weakly stained with Sirius red and not segmented by Kurita's method.

3.1.3. Morphologic filtering algorithm

An original algorithm was designed to extract IMCT from thresholded image elements. In the interstitial region

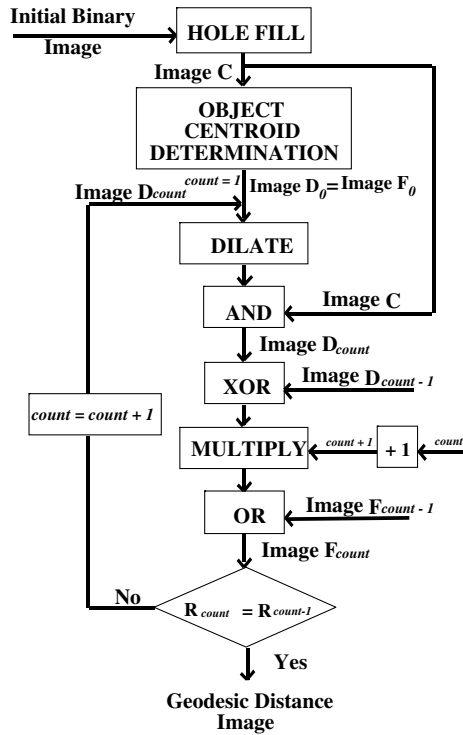


Fig. 2. Flow chart of the algorithm used to determine geodesic length, iteratively combining logical and mathematical morphology operations on the binary image.

of the image, areas of IMCT were identified as those elements with surface area $> 35\mu\text{m}^2$. Smaller elongated IMCT areas were separated from round muscle cell nuclei by using dilation and “hit or miss” and Boolean operations, and were classified as elongated objects when they had a “geodesic length” of more than 13 pixels ($\approx 11\ \mu\text{m}$) (Fig. 2).

The geodesic length was determined by means of an algorithm that iteratively combined logical and mathematical morphology operations on the binary image representing the mask of the elements contained in the image (Fig. 3). The algorithm initially determined the centroids of the objects in the image and successively, by iteration of logical operations and dilation, the centroids were dilated by reconstructing the initial objects and producing an image in which each pixel of each isolated element was assigned a grey level equal to the geodesic distance between that pixel and the pixel furthest from the same element. Centroids of objects were determined by iteratively applying the “Thinning” mathematical morphology operation to the binary images of the objects until convergence (i.e., until no modifications in the resulting image were produced between two successive iterations) and by using elements representing the so-called D configuration in all possible rotations as structural elements. Hole-filling was obtained iteratively by using the negative of the negative image of the objects without holes according to the sequence “Dilation” and “And” applied to the image frame and negative of the initial image with holes (Fig. 4).

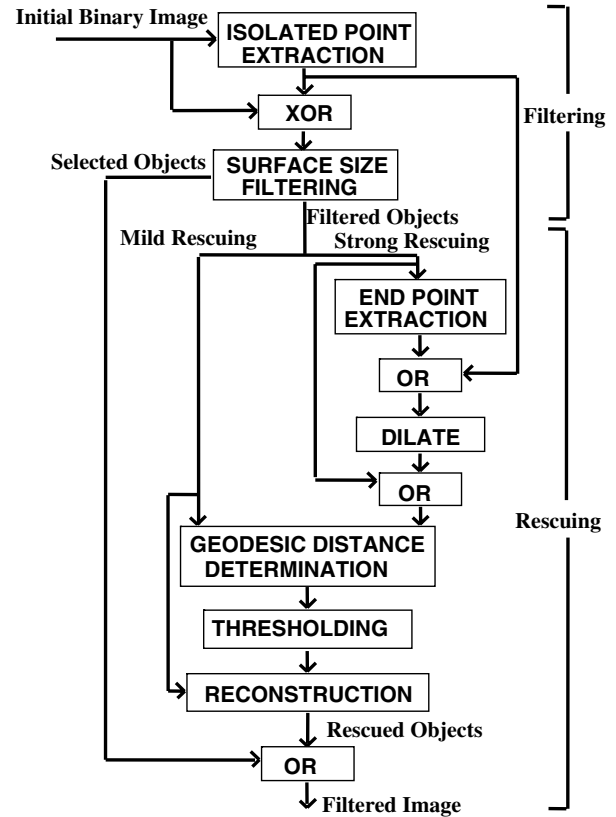


Fig. 3. Flow chart of the algorithm implemented for the geodesic length (see text).

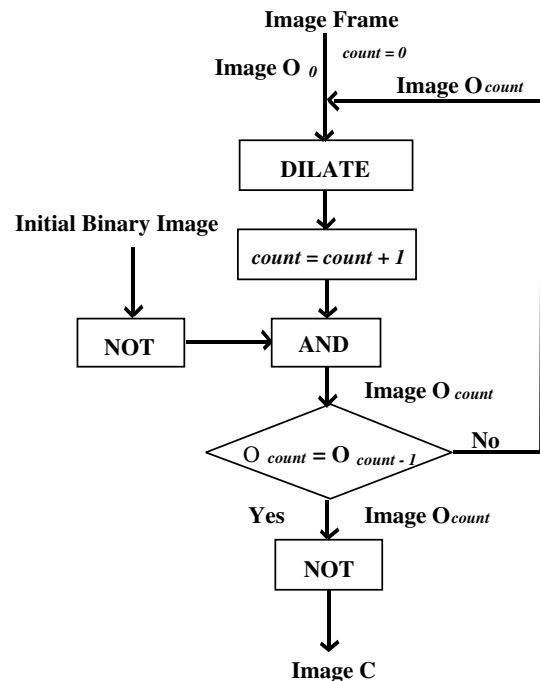


Fig. 4. Flow chart of the hole-filling module. Hole-filling was obtained iteratively by using the negative of the negative image of the objects without holes according to the sequence “Dilation” and “And” applied to the image frame and negative of the initial image with holes.

3.1.4. IMCT area identification

IMCT was identified using an automatic mathematical morphology algorithm. Initially, the binary image comple-

ment of the previously thresholded areas was automatically processed by a sequence of mathematical morphology “hit or miss” transformations (Fig. 5).

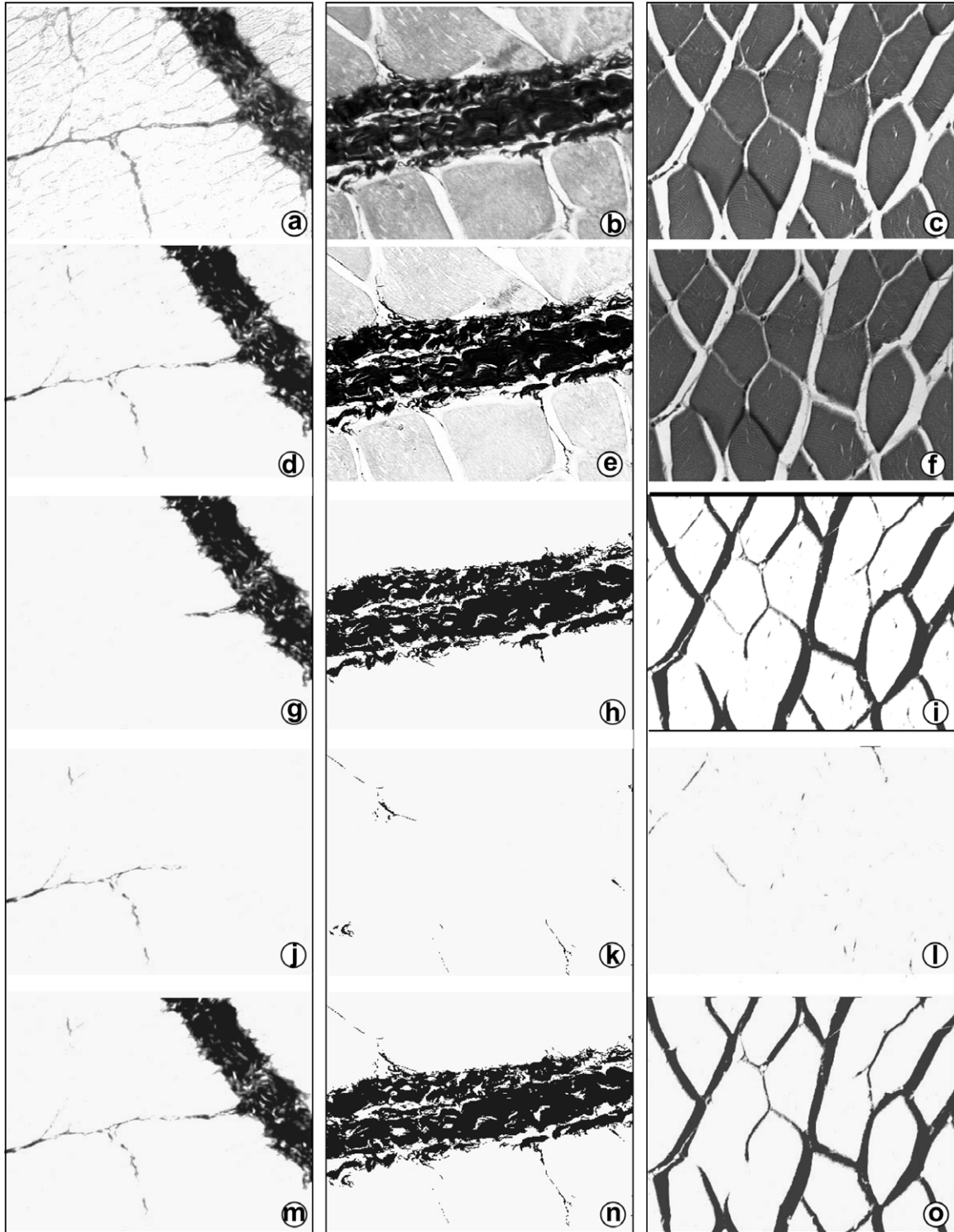


Fig. 5. Phases of image analysis process. (a) Digital image for quantification of IMCT of the meat (Sirius red 10×). (b) Digital image for quantification of *perimysium* (Sirius red 20×). (c) Digital image for quantification of muscle fibre retraction (hematoxylin–eosin 20×). (d–f) Images normalized and improved using the computer application. (g–i) Binary images; the area of interest is in black. (j–l) Images resulting from the application of the filtering and reconstruction algorithms corresponding to elements extracted from connective tissue areas in the thresholded image and added to images g, h, and i, respectively. (m) Area of IMCT. (n) Area of *perimysium*. (o) Area of muscle fibre retraction to be quantified.

3.1.5. Fibre retraction

The total area occupying the area is calculated by the software. Muscle fibre retraction is quantified on the negative of the hematoxylin–eosin-stained images.

3.1.6. Image analysis

Segmented image elements of interest were quantified in μm^2 , and the percentage area of IMCT was calculated as follows: $\text{IMCT} = 100 \times \text{CA}/\text{IA}$, where CA is the connective area, and IA is the area of the whole image.

3.1.7. Algorithm training

For the training of the algorithm, 300 images were used to determine the optimal microscope condenser aperture settings for the capture and digitalization of images and the image analysis. The images were visually evaluated and also automatically quantified, determining the % connective tissue area. Tukey's penalization and the Newman–Keuls method was used for multiple comparisons between mean values of pairs of images captured with the same diaphragm aperture, finding no significant differences in evaluations with apertures between positions 1.5 and 6 ($p > 0.1$). These evaluations were repeated after an interval of several days and the results of both were analysed by calculating the percentage of intra- and interobserver agreement in the determination of optimum aperture range, finding no significant differences.

3.1.8. Software validation

Our group previously developed and validated applications based on the same methodology and data processing to quantify interstitial fibrosis in liver and kidney (Masseroli et al., 2000; Masseroli et al., 1998). The robustness of the nonlinear image processing algorithms used was demonstrated by the evaluation of images experimentally perturbed to simulate slight progressive increases and decreases in stained areas. Quantifications of different areas showed strong correlations with the degree of image perturbation. The values were distributed in an almost linear manner, with small oscillations due mainly to the automatic thresholding algorithm. These fluctuations produced differences in histologic quantifications, but these were within the limits of precision of available tissue sectioning and staining techniques. Similarly, Sirius red staining was chosen for its reproducibility and stability and its virtual absence of artefacts and background. Moreover, the possible intra- and inter-observer variability was tested with different statistical tests, obtaining an intra-observer agreement of $>95\%$ and inter-observer agreement of $>90\%$. The lack of a standard for tissue staining intensity prevents the automatic normalization of image acquisition illumination according to this parameter, so that any possible batch differences in staining intensity can be compensated only by the interactive tuning of image acquisition illumination. This practice can lead to inter-assay differences that bias the reproducibility and objectivity of quantifications. Digital image normalization and the use of our

acquisition control function ensure the total intra-observer reproducibility of image acquisition illumination settings. The efficacy of acquisition control function in improving the objectivity and reproducibility of condenser aperture setting was tested by repeating the visual evaluation of the same images using the control function. The intra- and interoperator reproducibility of the acquisition illumination was validated in a study by Masseroli et al. (1998), based on visual evaluations by four expert independent observers. Each observer twice defined the range of microscope condenser apertures that gave images with the most appropriate intensity for subsequent automatic evaluation. The same images were also automatically evaluated to determine the range of microscope condenser apertures that gave quantifications that did not differ significantly. To assess the accuracy of the proposed automatic method, values of connective tissue obtained in the same images by means of Kurita et al.'s (1992) automatic thresholding were compared with manual thresholding reference values and the results of three other global automatic thresholding methods: Kittler and Illingworth's method with Gaussian distribution of gray levels (1986), Kittler and Illingworth's with Poisson's distribution of gray levels, and the corrected isodata method. The present programme uses similar conditions of capture and the same logical operations, mathematical morphology, and image analysis as but was specifically designed to study meat tissue parameters.

3.2. Application

Several authors have reported a good correlation between imaging analysis and biochemical hydroxyproline determination in the quantification of collagen, confirming the accuracy of the former approach (Kalaria & Pax, 1995; Nicoletti et al., 1996; Sifre et al., 2005; Sifre-Maunier et al., 2006). Compared with conventional methods, imaging analysis yields additional information on parameters related to the arrangement and architecture of IMCT that could not previously be evaluated, besides providing a more precise quantification of standard variables.

Table 1 lists the means and statistical significance of morphometric parameters analyzed in meat of the different species. Statistically significant differences were found in the percentage and area occupied by IMCT among the different muscles and animal species studied ($p < 0.001$, Kruskal–Wallis). M of Rubia Gallega beef had the largest area of IMCT ($p = 0.009$, Mann–Whitney U test), followed by LT of Iberian pork, LT of lamb, TB of lamb, LT of Kobe beef, PM of pigeon and LT of Rubia Gallega beef.

Data on the % of total collagen area occupied by *perimysium* in LT obtained by Nakamura et al. (2003) in castrated male pigs ((Landrace \times Duroc) $\text{♀} \times$ Duroc ♂) were relatively similar ($25.4\% \pm 0.9$ in type I collagen and $37.6\% \pm 1.0$ in type III collagen) to the present observations in Large White crossbreed pigs (% *perimysium* 22.59 ± 0.87) despite the different histologic technique and different magnifications used ($2\times$ by Nakamura et al.

Table 1
Morphometric parameters in the different meat tissues studied using the digital image analysis application

Parameters	<i>Triceps brachii</i> (Lamb)	<i>Longissimus thoracis</i> (Lamb)	<i>Massetter</i> (<i>Bos taurus</i> Rubia Gallega beef)	<i>Longissimus thoracis taurus</i> Rubia Gallega beef)	<i>Pectoralis it major</i> (Pigeon)	<i>Longissimus thoracis</i> (Kobe beef)	<i>Longissimus thoracis</i> (Iberian pork)	<i>Longissimus thoracis</i> (Large white crossbreed pork)	<i>P</i> value
% IMCT (μm^2)	7.53 ± 1.95	8.43 ± 4.29	28.75 ± 10.63	3.20 ± 0.98	4.11 ± 2.24	4.37 ± 1.20	17.02 ± 14.99	4.00 ± 2.15	0.001
IMCT (μm^2)	4530.96 ± 1173.79	5070.49 ± 2580.10	17293.49 ± 6393.30	1926.39 ± 587.88	2476.28 ± 1340.45	2627.47 ± 725.46	10238.13 ± 9014.84	2406.11 ± 1294.70	0.001
% <i>Perimysium</i>	13.78 ± 4.21	20.65 ± 1.50	75.07 ± 17.10	3.00 ± 2.11	7.66 ± 1.17	5.82 ± 2.81	9.93 ± 4.95	22.59 ± 0.87	0.001
<i>Perimysium</i> area (μm^2)	8289.90 ± 2533.18	12419.74 ± 902.70	45150.30 ± 10283.31	1804.18 ± 1267.05	4609.27 ± 705.28	3498.74 ± 1693.511	5971.09 ± 2974.71	13587.70 ± 521.79	0.001
% Fiber retraction	13.27 ± 2.81	3.16 ± 2.30	11.86 ± 3.40	17.12 ± 1.67	11.52 ± 2.34	22.69 ± 0.30	20.16 ± 3.08	13.45 ± 3.69	0.001
Area fiber retraction (μm^2)	52163.38 ± 1688.13	58243.26 ± 1383.28	53014.37 ± 2048.37	49847.73 ± 1008.06	53.218.26 ± 1408.31	46495.47 ± 181.11	48020.55 ± 1853.97	52053.50 ± 2216.58	0.001

Mean ± standard deviation.

versus 20× in the present study). The question arises as to whether IMCT is a fractal system.

Two recent studies (Sifre et al., 2005; Sifre-Maunier et al., 2006) used the same histologic technique as the present study (Sirius red staining), although they used cryopreserved rather than paraffin-embedded samples. Both studies stained IMCT collagen in LT with Sirius red, applying a green optical filter to improve the contrast and using Visilog software for image analysis. The only difference between the present research and these studies was the observation scale and breeds of animal studied. Thus, they acquired images at 2× magnification, whereas we used 10× magnification for IMCT and 20× magnification for *perimysium* and fibre retraction.

In studies of the % of total muscle area occupied by IMCT, Sifre et al. (2005) reported a % IMCT of 2.8 ± 0.4 (threshold confidence level (ϵ) of 0.80) in LT of 5-year-old Charolais cull cows and Sifre-Maunier et al. (2006) % IMCT values of 3.1 and 14.0 in LT of 3–7-year-old Charolais cows for ϵ values of 0.80 and 0.55, respectively. We found % IMCT of 3.20 ± 0.98 in LT of Rubia Gallega cows (450 kg) and 4.37 ± 1.20 in Kobe beef (550–570 kg). Our findings in Rubia Gallega cows were in agreement with those reported by Sifre et al. (2005) and Sifre-Maunier et al. (2006), despite the use of different observation scales. These results again raise the question as to whether IMCT is a fractal system. It is highly probable that the greater presence of IMCT in Kobe beef is due to the higher age of these animals and their diet.

Perimysium size also significantly differed among the different muscles ($p < 0.001$, Kruskal–Wallis). The area occupied by the *perimysium* was significantly larger in M of Rubia Gallega beef compared with the other samples ($p < 0.05$, Mann–Whitney *U* test) and was smallest in LT of Kobe beef ($p < 0.05$, Mann–Whitney *U* test). We found statistically significant differences in Sirius red-stained meat tissue (LT) between Large White crossbreed and Iberian pigs. Iberian pork had a higher % IMCT (17.02 ± 14.99 versus 4.00 ± 2.15 ; $p = 0.028$, Mann–Whitney *U* test), whereas the Large White pork presented a higher % *perimysium* (22.59 ± 0.87 versus 9.93 ± 4.95 ; $p = 0.009$, Mann–Whitney *U* test).

Significant differences species in the degree of muscle fibre retraction were observed among the different animals ($p < 0.001$, Kruskal–Wallis). The greatest degree of retraction was observed in LT of Kobe beef and the least in LT of lamb. Significant differences were also found among different muscles in the same species ($p < 0.05$, Mann–Whitney *U* test). The degree of retraction was not correlated with the area of IMCT or *perimysium* in any sample studied (non-significant Spearman's ρ).

Sifre et al. (2005), using an adaptive thresholding method based on probabilistic maps and a confidence level (degree-of-freedom of the algorithm) of 80%, reported that models were less efficient when segmentation extracting the thinner network was performed (lower confidence level; $\epsilon = 40\%$). Sifre-Maunier et al. (2006) used probabilistic

map thresholding (PMT) and found a wide variability in results according to the confidence level used (ε) to determine the optimal threshold. At high confidence (ε) levels (70%, 75%, and 80%), corresponding to the thick network, the standard error was increased (to >3 gray levels); at low ε levels, the thickness of secondary segments (thinnest segments) was over-estimated (Sifre-Maunier et al., 2006). They reported that PMT thresholding rules depend on the ε level, whereas Rosin's thresholding algorithm and Otsu's algorithm are only adaptive to the image context and give a single threshold value regardless of the ε value (Sifre-Maunier et al., 2006). Pir application, based on a modification of Otsu's algorithm, gives a single threshold value, which we consider essential for intra- and interobserver reliability and the reproducibility of results. Sifre-Maunier et al. (2006) found that Rosin's thresholding algorithm and Otsu's algorithm did not take account of the thinnest segments, which were segmented at confidence levels below 70%. This error was corrected by applying a second algorithm using Kittler and Illingworth thresholding (Kittler & Illingworth, 1986). This was implemented on the initial image to detect lower grey levels and isolate weakly stained areas not segmented by Kurita's method. Sifre-Maunier et al. (2006) concluded that the limiting factor of the PMT method is the learning step to build the thresholding rules, which must be changed for every modification of acquisition conditions. In our software, the digital image normalization and acquisition control function ensure total intra-observer reproducibility of image acquisition conditions, and the present study validated the efficacy of the acquisition control function in improving the objectivity and reproducibility of condenser aperture setting. Sifre-Maunier et al. (2006) confirmed the high sensitivity of the PMT method to a heterogeneous background at low ε , since it selects lighter grey levels to obtain thinner segments and therefore tends to binarize false background noise. Our software corrects for this potential problem by comparing the image pixel-by-pixel with a previously acquired background image and producing a corrected image.

In the study by Sifre-Maunier et al. (2006), 20 non-trained judges drew what they thought to be IMCT by using a one-pixel-thick black line. The intra- and interoperator reproducibility was validated in the present study by using four independent expert observers, who showed no significant differences in results ($p < 0.05$; Masseroli et al., 1998). Sifre-Maunier et al. (2006) concluded that non-expert judges could be trained to produce more consensual drawings.

The meat of the different animals presented highly similar gross features but showed clear microscopic differences. It is widely accepted that organoleptic (especially textural) variability among different animal meats can mainly be explained by differences in the composition and arrangement of muscle fibres and IMCT. Meat quality attributes such as meat colour, marbling, maturity, IMCT and meat texture can be effectively quantified and predicted to a sat-

isfactory degree-of-accuracy. Image processing has been used to assess beef quality in terms of the percentage of marbling area, using morphological operations to separate connected meat tissues and measure the marbling area. However, research has shown that marbling and colour characteristics only explain a rather low percentage of the variations in important palatability measures such as tenderness (Li, Tan, Martz, & Heymann, 1999; Li, Tan, & Shatadal, 2001). Wheeler et al. (2002) concluded that non-invasive methods to predict meat tenderness based primarily on lean colour may not be sufficiently accurate to warrant their use. IMCT quantity and spatial distribution, which define the grain of meat, are of great importance among the multiple meat tissue characteristics that influence meat quality because they are directly related to its tenderness (Lepetit & Culioli, 1994). Thus, there is a clear correlation between total collagen content and muscle toughness and a high positive correlation between Warner-Bratzler Shear Force and total collagen content ($r = 0.723$; $p < 0.01$; Torrescano et al., 2003).

New methods are required to predict meat tenderness and classify meat type, breed, and age in order to accurately identify beef that can be guaranteed to be tender. Although further studies are required, these findings indicate that automatic image analysis of microscopy sections is a highly promising and versatile method to discriminate the components of a given tissue.

4. Conclusion

This image analysis application permits the automatic, accurate, objective and reliable quantification of IMCT and fibre retraction in muscle. It can analyze 20 images per min and offers more precise measurements compared with conventional morphometric methods. Changes in the physicochemical properties of meat have a histologic basis. Variations in the proportion of IMCT, the greater or lesser retraction of muscle fibres, loss of water from the tissue and/or the degree of cell autolysis can modify the organoleptic characteristics of meat. The use of the present technique to precisely quantify these parameters will help to increase understanding of these relationships and enable study of the architecture and IMCT of meat for clarifying tissue changes that result from different storage, refrigeration, freezing and cooking conditions.

Acknowledgements

We especially acknowledge the contribution of María Dolores Rodríguez, Francisca Sáez and Mercedes García-Román, technicians at the Department of Pathology. Special thanks to Andoni Luis Adúriz, Chef of Mugaritz Restaurant (Guipúzcoa, Spain), for his collaboration in this paper. This work was funded by the Corporación Tecnológica de Andalucía.

References

- Cross, H. R., Gilliland, D. A., Durland, P. R., & Seideman, S. (1983). Beef carcass evaluation by use of a video image analysis system. *Journal of Animal Science*, 57(4), 910–917.
- Du, C., & Sun, D. (2004). Shape extraction and classification of pizza base using computer vision. *Journal of Food Engineering*, 64, 489–496.
- Kalaria, R. N., & Pax, A. B. (1995). Increased collagen content of cerebral microvessels in Alzheimer's disease. *Brain Research*, 705, 349–352.
- Kittler, J., & Illingworth, J. (1986). Minimum error thresholding. *Pattern Recognition*, 19, 41–47.
- Kurita, T., Otsu, N., & Abdelmalek, N. (1992). Maximum likelihood thresholding based on population mixture models. *Pattern Recognition*, 25, 1231–1240.
- Lepetit, J., & Culioli, J. (1994). Mechanical properties of meat. *Meat Science*, 36, 203–237.
- Li, J., Tan, J., Martz, F., & Heymann, H. (1999). Image texture feature as indicators of beef tenderness. *Meat Science*, 53, 17–22.
- Li, J., Tan, J., & Shatadal, P. (2001). Classification of tough and tender beef by image texture analysis. *Meat Science*, 57, 341–346.
- Masseroli, M., Caballero, T., O'Valle, F., Del Moral, R. M., Pérez-Milena, A., & Del Moral, R. G. (2000). Automatic quantification of liver fibrosis: design and validation of a new image analysis method: comparison with semi-quantitative indexes of fibrosis. *Journal of Hepatology*, 32(3), 453–464.
- Masseroli, M., O'Valle, F., Andújar, M., Ramírez, C., Gómez-Morales, M., de Dios Luna, J., et al. (1998). Design and validation of a new image analysis method for automatic quantification of interstitial fibrosis and glomerular morphometry. *Laboratory Investigation*, 78(5), 511–522.
- Nakamura, Y. N., Iwamoto, H., Ono, Y., Shiba, N., Nishimura, S., & Tabata, S. (2003). Relationship among collagen amount, distribution and architecture in the *M. longissimus thoracis* and *M. pectoralis profundus* from pigs. *Meat Science*, 64, 43–50.
- Nicoletti, A., Heudes, D., Mandet, C., Hinglais, N., Bariety, J., & Michel, J. B. (1996). Inflammatory cells and myocardial fibrosis: spatial and temporal distribution in renovascular hypertensive rats. *Cardiovascular Research*, 32(6), 1096–1107.
- Ötles, S., & Önal, A. (2004). Computer-aided engineering software in the food industry. *Journal of Food Engineering*, 65, 311–315.
- Purslow, P. P. (2005). Intramuscular connective tissue and its role in meat quality – review. *Meat Science*, 70, 435–447.
- Sifre, L., Berge, P., Engel, E., Martin, J. F., Bonny, J. M., Listrat, A., et al. (2005). Influence of the spatial organization of the perimysium on beef tenderness. *Journal of Agricultural and Food Chemistry*, 53, 8390–8399.
- Sifre-Maunier, L., Taylor, R. G., Berge, P., Culioli, J., & Bonny, J. M. (2006). A global unimodal thresholding based on probabilistic reference maps for the segmentation of muscle images. *Image and Vision Computing*, 24, 1080–1089.
- Swatland, H. J. (1995). Objective assessment of meat yield and quality. *Trends in Food Sciences and Technology*, 6, 117–120.
- Swatland, H. J. (2006). Stratification of connective tissue toughness in beef roasts assessed by simultaneous fluorometry and penetrometry. *Food Research International*, 39, 1106–1109.
- Sweat, F., Puchtler, H., & Rosenthal, S. I. (1964). Sirius red F3BA as a stain for connective tissue. *Archives of Pathology*, 78, 69–72.
- Tan, J. (2004). Meat quality evaluation by computer vision. *Journal of Food Engineering*, 61, 27–35.
- Vote, D. J., Belk, K. E., Tatum, J. D., Scanga, J. A., & Smith, G. C. (2003). Online prediction of beef tenderness using a computer vision system equipped with a BeefCam module1. *Journal of Animal Science*, 81, 457–465.
- Wassemberg, R. L., Allen, D. M., & Kemp, K. E. (1986). Video image analysis prediction of total kilograms and percent primal lean and fat yield of beef carcasses. *Journal of Animal Science*, 62(6), 1609–1616.
- Wheeler, T. L., Vote, D., Leheska, J. M., Shackelford, S. D., Belk, K. E., Wulf, D. M., et al. (2002). The efficacy of three objective systems for identifying beef cuts that can be guaranteed tender. *Journal of Animal Science*, 80, 3315–3327.
- Wyle, A. M., Vote, D. J., Roeber, D. L., Cannell, R. C., Belk, K. E., Scanga, J. A., et al. (2003). Effectiveness of the SmartMV prototype BeefCam System to sort beef carcasses into expected palatability groups. *Journal Animal of Science*, 81, 441–448.